CORNELL UNIVERSITY MATHEMATICS DEPARTMENT SENIOR THESIS

Orthogonal Polynomials with Respect to Self-Similar Measures

A THESIS PRESENTED IN PARTIAL FULFILLMENT
OF CRITERIA FOR HONORS IN MATHEMATICS

Philip Daniel Owrutsky

May 2006

BACHELOR OF ARTS, CORNELL UNIVERSITY

THESIS ADVISOR(S)

Robert Strichartz
Department of Mathematics

Orthogonal Polynomials with Respect to Self-Similar Measures

Honors Thesis

Philip Owrutsky [1]
Math Dept, Malott Hall
Cornell University
Ithaca NY, 14853
pdo4@cornell.edu,

Introduction

Driven by various applications, the development of sets of functions that are orthonormal with respect to weighted integration ($\int_I W(x) f_i(x) f_j(x) dx = \delta_{ij}(x)$) have been well studied throughout history. In particular, a variety of such orthogonal polynomials have been developed with applications ranging from numerical integration to solutions of the harmonic oscillator. It can be shown that all sets of orthogonal polynomials obey a 3-term recursion[SZ]:

$$xP_j(x) = r_{j+1}P_{j+1}(x) + A_j P_j(x) + r_j P_{j-1}(x) \tag{1}$$

for certain coeffecients $r_j, A_j \epsilon \Re$

Advances in numerical methods have produced stable techniques for computing the coefficients of the 3-term recursion formula for a wide variety of weighting functions[M1-2]. In fact the notion of orthonormal can be generalized to

$$\int f_i(x) f_j(x) d\mu = \delta_{ij} \tag{2}$$

where μ is a measure.

In this paper we deal with a special case of self-similar measures. These Self-similar measures satisfy:

$$\int f(x) d\mu(x) = P \int f\left(\frac{1}{R}\right) d\mu(x) + (1-P) \int f\left(\frac{1}{R}x + 1 - \frac{1}{R}\right) \tag{3}$$

This paper analyzes two such extensions; orthogonal polynomials with respect to the standard Cantor measure (hereon called Cantor Legendre Polynomials) which corresponds to $P = 1/2$ and $R > 2$ in (3) as well as orthogonal polynomials with respect to a particular non-uniform weighting of the unit interval (later called Weighted Legendre Polynomials) with $P \neq 1/2$ and $R = 2$. We use the method and codes of Giorgio Mantica to compute the coefficients in the 3-term recursion relation.

[1] Cornell Presidential Research Scholar

Cantor Legendre

The Cantor set is a subset of the real line with Lebesgue measure zero (has no length in the traditional sense). The original Cantor set was formed by removing the middle third of line segments. The first step removes the middle third from the unit interval. Then the middle third of the 2 remaining line segments are removed. This process is continued ad infinitum. This paper will use a general Cantor set that takes an input parameter R that will determine the scale of the set. Then apply

$$C_1 = \frac{1}{R}(0,1) \bigcup \left(\frac{1}{R}(0,1) + (1 - \frac{1}{R}) \right) \tag{4}$$

This will remove the middle $1 - 2/R$ of the unit interval. A Cantor set is obtained by iterating this process:

$$\begin{aligned} C_2 &= \frac{1}{R}C_1 \bigcup \left(\frac{1}{R}C_1 + (1 - \frac{1}{R}) \right) \\ C_n &= \frac{1}{R}C_{n-1} \bigcup \left(\frac{1}{R}C_{n-1} + (1 - \frac{1}{R}) \right) \end{aligned}$$

Note that this reduces to the original Cantor set when R=3.

To see that this construction produces something with Lebesgue measure zero, observe that $C_0 = (0,1)$ has measure (length) 1, and that C_1 has measure $1 - 2/R$ (this is precisely how much was removed). By analogy C_2 has measure $(1 - 2/R)^2$, and in general C_n has measure $(1 - 2/R)^n$. As n tends to infinity: $\lim_{n\to\infty}(1 - 2/R)^n = 0$. Since the Cantor set has zero measure, we must adopt a meaningful notion of the integral for the set. We will use the following (normalized Hausdorf measure):

$$\int_\mu f_i(x) f_j(x) d\mu = \lim_{m\to\infty} 1/m \sum_{k=0}^{m} f_i(x_k) f_j(x_k) \tag{5}$$

where $\{x_i\}$ is a discrete approximation of the Cantor set

In order to make the construction of the Cantor set amenable to a computer, we will follow the iterative scheme outlined above, but truncate after 12 iterations producing an approximate Cantor set containing 2^{13} points. This will transform (4) into:

$$\int_\mu f_i(x) f_j(x) d\mu = \frac{1}{2^{13}} \sum_{k=0}^{2^{13}} f_i(x_k) f_j(x_k) \tag{6}$$

Also, to make visualizing the graphs easier (rather than a plot of points) we will conduct all calculations on the truncated Cantor Set, but plot against a Distorted Cantor Set. The Distorted Cantor construction will take ϵ and R as inputs and construct a modified Cantor set that has center gap ϵ, secondary gap ϵ/R and tertiary gaps of size ϵ/R^n where n is the iteration in which the gap is constructed.

The advantage to the Distorted Cantor set is that it has finite length (even in the event that it

is not truncated), while maintaining the characteristic structure of a Cantor Set (there is a one to one correspondence between points in a Cantor and points in a Distorted Cantor). This will make plots more easily understood.

Weighted Legendre

A common set of Orthogonal Polynomials are the Legendre Polynomials. These are usually defined on the interval $(-1, 1)$, but can also be formulated on the interval (0,1). We can use the scheme outlined above to produce the traditional Legendre Polynomials on the interval (0,1) by letting R=2. In this case there is no gap and the unit interval is preserved.

A logical extension to the R=2 case involves modifying the weighting of the two half intervals. For example, the left half interval could be assigned 70 percent of the total measure while the right half would only receive 30 percent. Successive iterations produce a non-uniform distribution of the measure on the unit interval, while maintaining a constant overall weight. As we will see, the resulting Orthogonal Polynomials (hereby called Weighted Legendre) share many of the properties of the original Legendre Polynomials.

This paper should be viewed in the context of a long term effort to understand topics in classical analysis extended to fractal measures. More data may be found at www.math.cornell.edu/~orthopoly

Discussion

Figures 1 and 2 display the advantages to plotting with a Distorted Cantor set. As plotted the curves resemble polynomials graphed on an interval that we are much more accustom to seeing.

Figure 4,5 and 6 show a rather unexpected property of the coefficients in the 3-term recurrence relation (eq. 1). Most of the odd indexed coefficients have value less than .2 while most of the even indexed coefficients have value greater than .3. In addition, there appears to a quasi-periodic structure to the values. Fast fourier transforms of the coefficients for large numbers of data points indicates that this may be quantifiable.

Figure 7 illustrates another property of the Cantor Legendre Polynomials (CLP). If we plot the CLPs on the entire interval we observe that they are roughly gaussian in the middle gap for $n \equiv 0, 2 \pmod 4$. Also, they are enormous in magnitude (10^{50}) while the polynomial when restricted to the Cantor set never exceeds a value of 20 for all $n < 2000$! Even more astonishing is that in the secondary gap (produced during the second iteration of the construction of the Cantor set) the CLPs are also

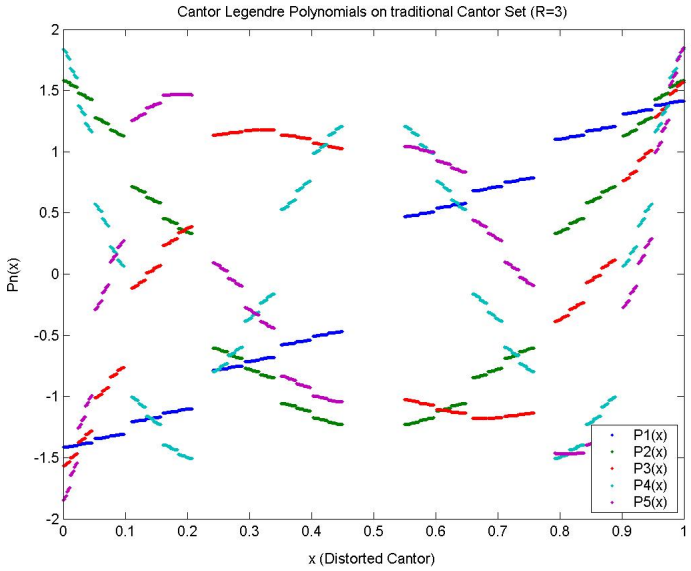

Figure 1: Plot of First 5 Cantor Legendre Polynomials for R=3

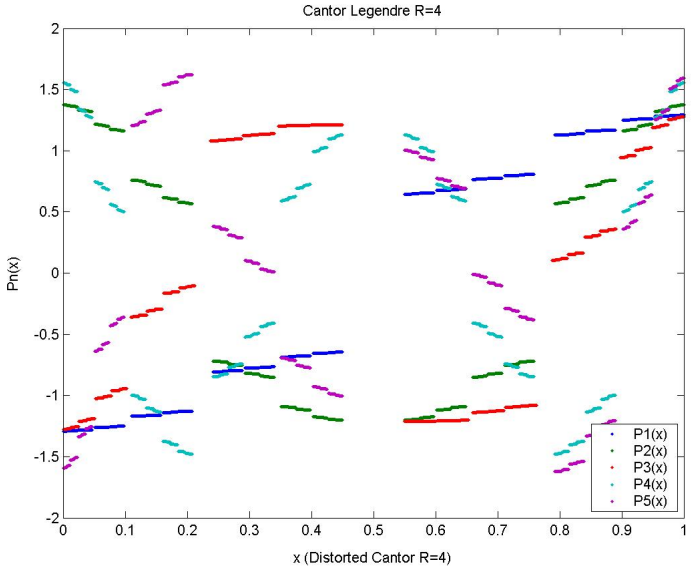

Figure 2: Plot of First 5 Cantor Legendre Polynomials for R=4

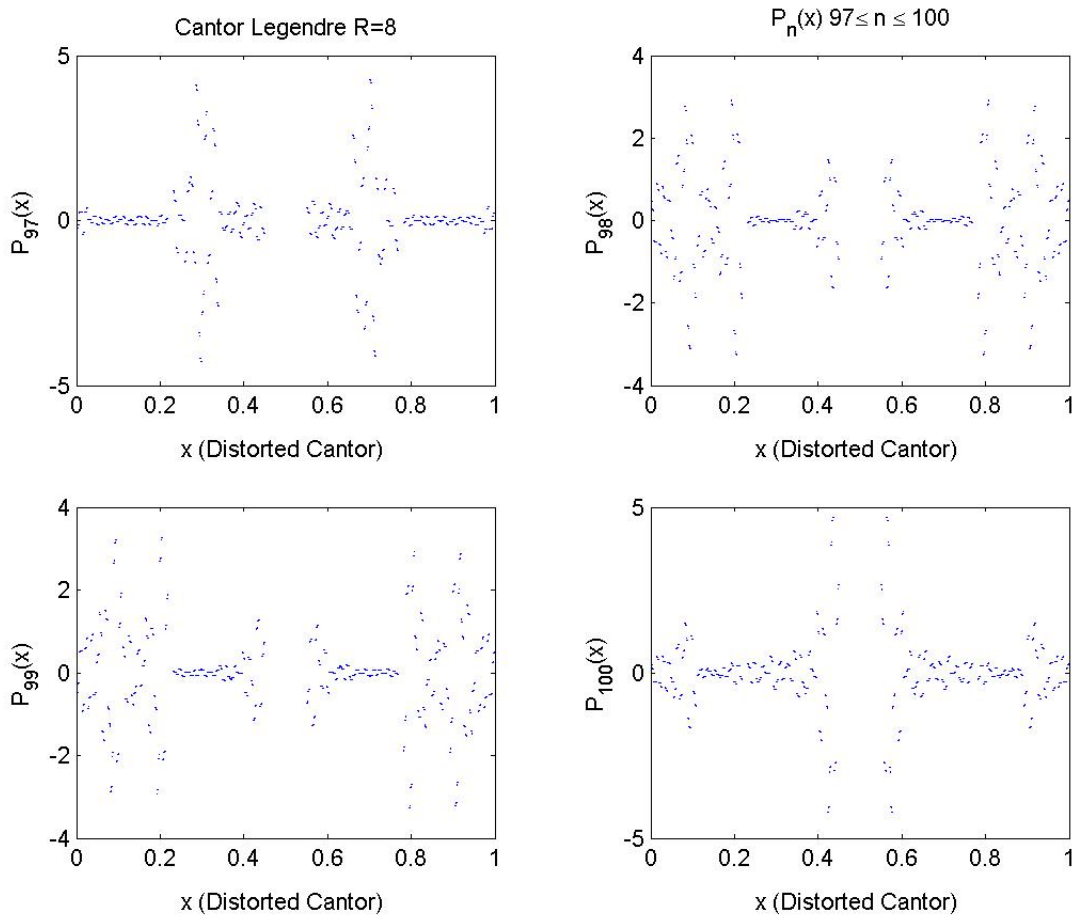

Figure 3: Plot of some larger n Cantor Legendre Polynomials with R=8; $97 \leq n \leq 100$

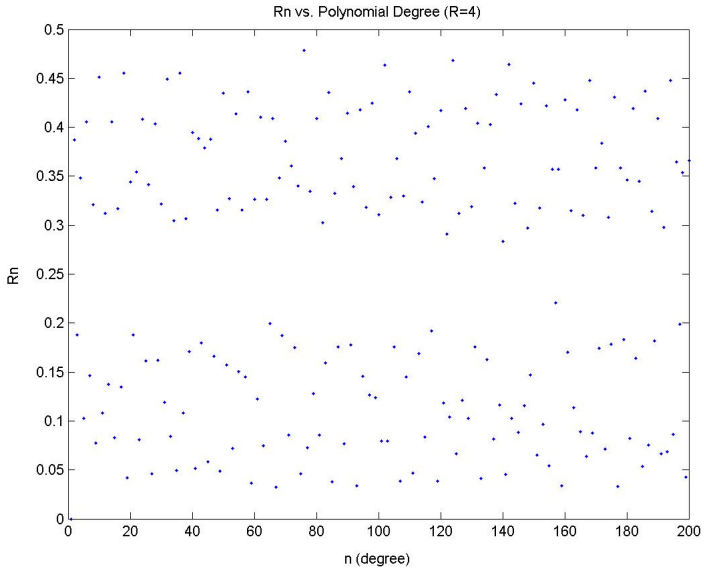

Figure 4: Plot of First 200 Rn Coefficients for R=4. Again all of the An's are 1/2 by symmetry. We continue to observe a quasi-periodic pattern to the Rn's and a stark contrast between even and odd values. This split occurred for most Rn for all tested values of R.

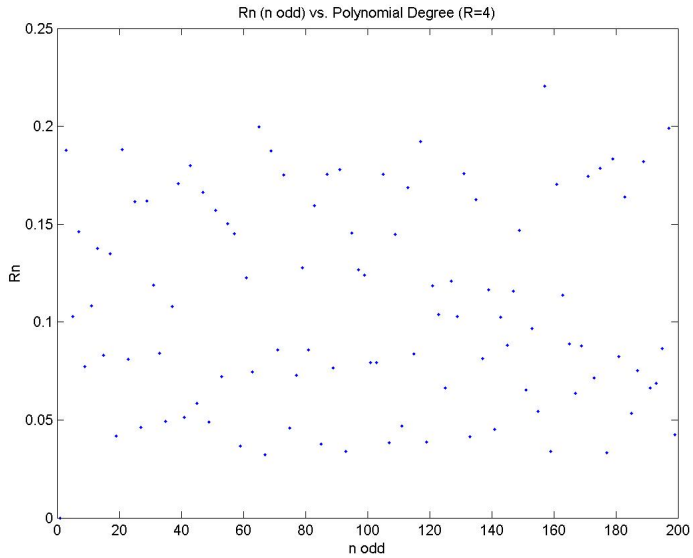

Figure 5: Plot of the first Rn Coefficients for R=4 and n odd. Again all of the An's are 1/2 by symmetry. We continue to observe a quasi-periodic pattern to the Rn's and a stark contrast between even and odd values. This split occurred for most Rn for all tested values of R.

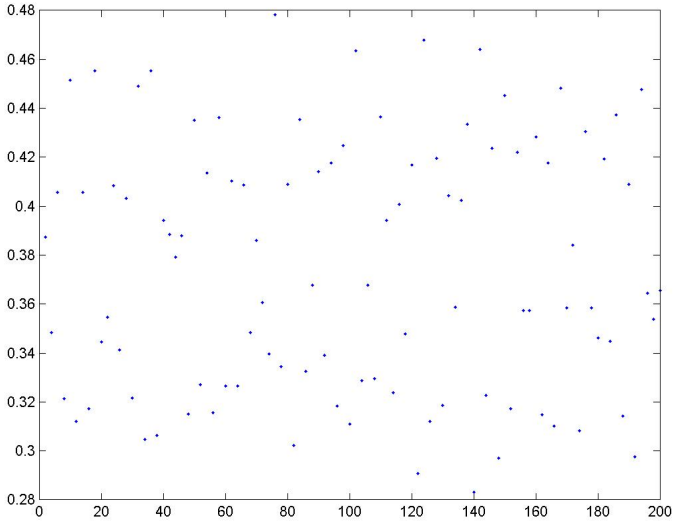

Figure 6: Plot of the first Rn Coefficients for R=4 and n even.

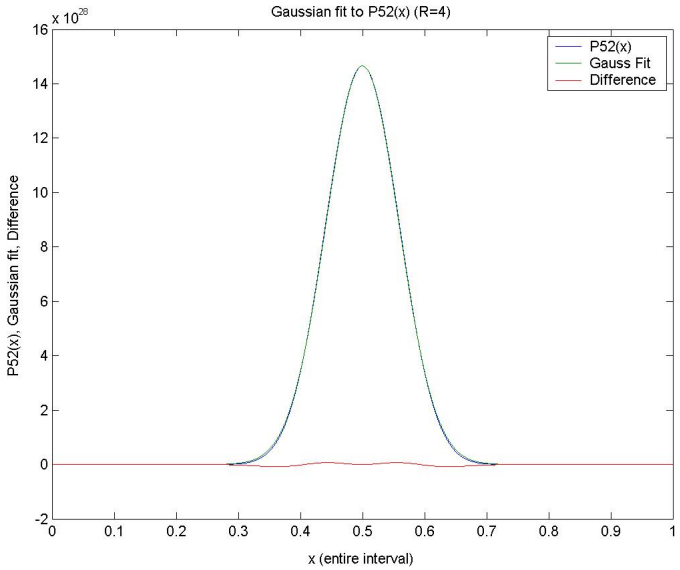

Figure 7: Plot of $P_{52}(x)$ on the entire interval. Notice the large value obtained by the polynomial off the Cantor Set (10^{28}) compared to never exceeding the value 10 on the Cantor Set ($\forall n |P_n| < 20$). The overall shape in the gap is also extremely Gaussian as indicated by the fit. $\forall n$ of the form $4k$ the center gap is approximately gaussian. For n of the form $4k + 2$ it is roughly a negative gaussian.

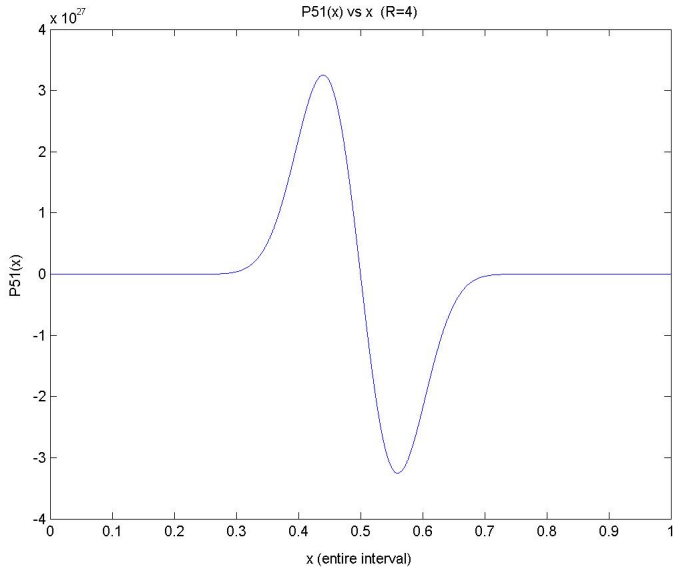

Figure 8: Plot of $P_{51}(x)$ on the entire interval. This is roughly the derivative of a Gaussian on the center gap. $\forall n$ of the form $4k+3$ we observe this shape, and for $4k+1$ we observe the negative.

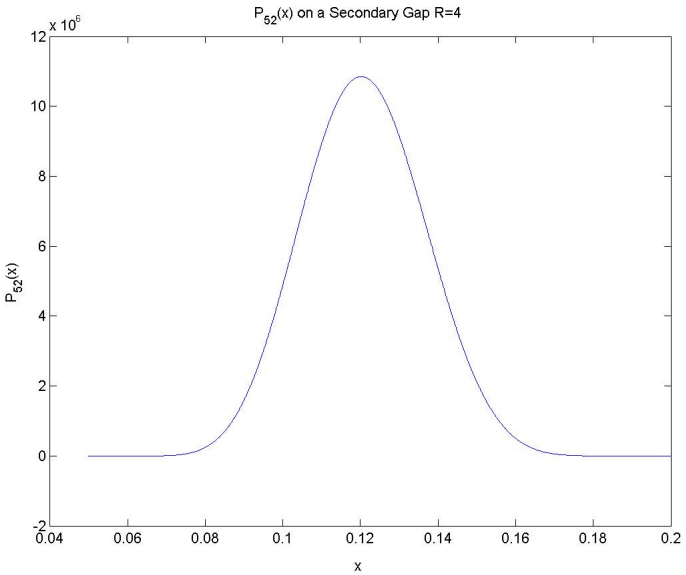

Figure 9: Plot of $P_{52}(x)$ on a secondary gap. Again we observe a gaussian shape.

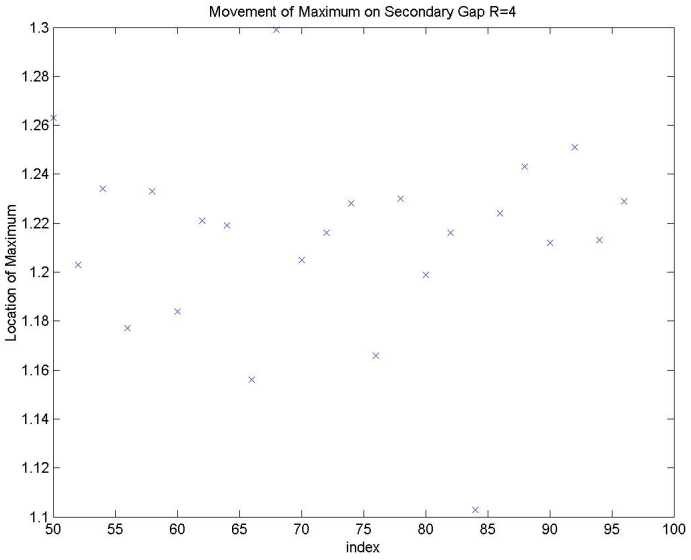

Figure 10: The center of the approximate gaussian in the secondary gap varies with index of the polynomial.

approximately gaussian. Figure 8 shows that for $n \equiv 1, 3 \pmod 4$ the CLPs are approximately the derivative of a Gaussian. Figure 10 shows that the center of the approximate Gaussian in the secondary gap is not constant, but varies with index. The actual center of the gap occurs at .125, but the center varies from roughly1.15 to 1.27, with the majority lying to the left of the actual center.
For large n, the odd indexed r_n are frequently quite small (as observed in figures 4 and 5) which causes $P_{2n} \cong P_{2n+1}$ on the right half of the Cantor set ($x > .5$) from the 3-term recursion relation. This approximate equality holds well for all $n > 30$ in the $R = 8$ case. Figure 11 shows an example of this.

The Dirichlet Kernel can be calculated using the defintion

$$DK_n(x, y) = \sum_{i=0}^{n} P_i(x)P_i(y) \tag{7}$$

where y is the center of the kernel. In the limit as n goes to infinity we are curious if DK_n will approach an approximate identity. Unfortunately, we were unable to confirm this for the CLPs. Figures 12 and 13 show Dirichlet Kernels for the R=3 and R=4 case. Although the shape greatly resembles an approximate identity, we were not able to confirm that the fluctuations away from the center were in fact tending to zero as n increased.

There is an alternative method for computing the Dirichlet Kernel. The Christoffel-Darboux identity states that:

$$DK_n(x, y) = \sum_{i=0}^{n} P_i(x)P_i(y) = \left(\frac{P_{n+1}(x)P_n(y) - P_n(x)P_{n+1}(y)}{x - y} \right) r_{n+1} \tag{8}$$

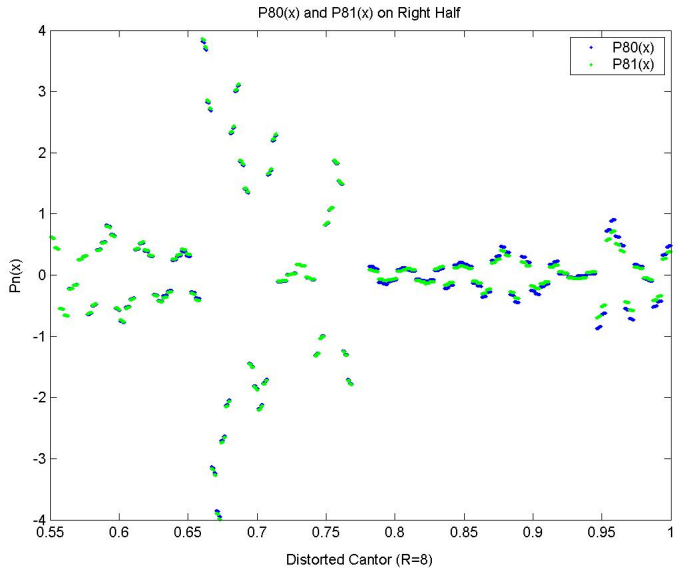

Figure 11: Plot of $P_{80}(x)$ and $P_{81}(x)$ with R=8 on the right half of the Cantor Set. Where the odd values of Rn are small, the recursion relation forces this approximate equality on the right half of the Cantor set. In general the odd Rn are small (especially compared to the even Rn).

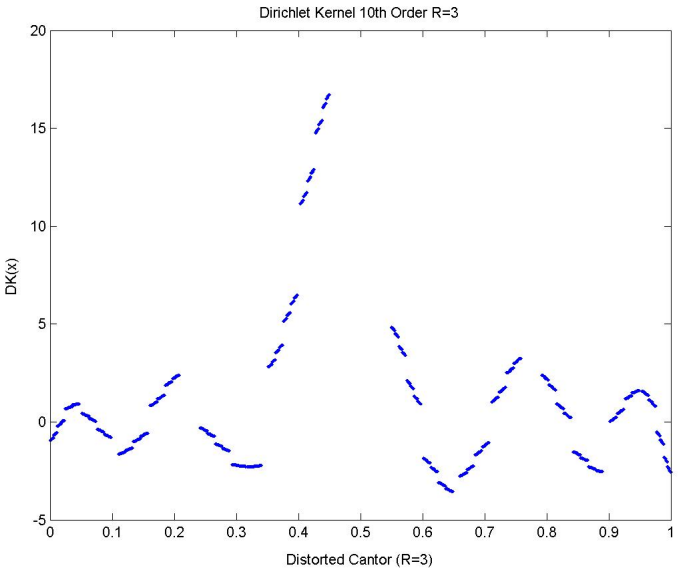

Figure 12: Plot of the Dirichlet Kernel for $R = 3$, $n = 10$ calculated using the definition of the kernel ($\sum_{i=0}^{n} P_i(x)P_i(y)$ where y is fixed as the right most point in the left half of the interval).

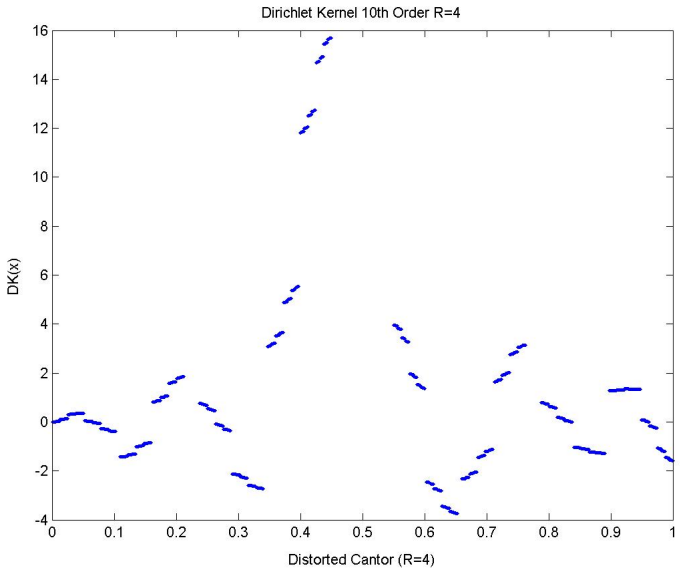

Figure 13: Plot of the Dirichlet Kernel for $R = 4$, $n = 10$ calculated using the definition of the kernel ($\sum_{i=0}^{n} P_i(x)P_i(y)$ where y is fixed as the right most point in the left half of the interval).

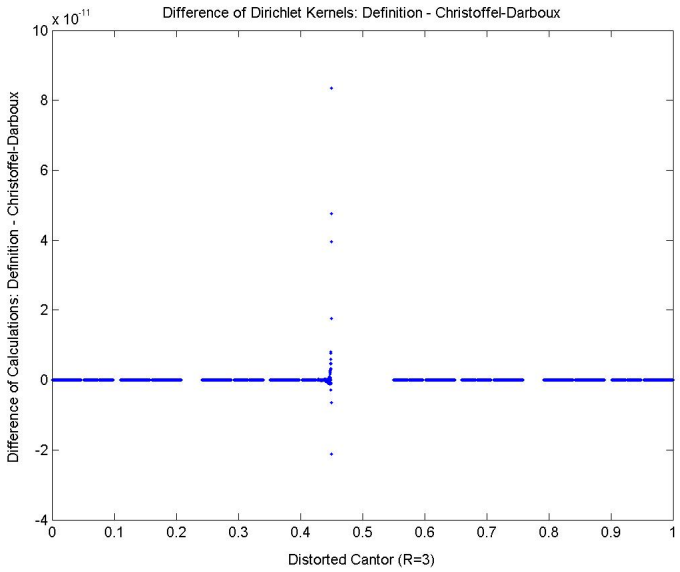

Figure 14: Plot of the difference in the Dirichlet Kernel for R=3 calculated using the definition and calculated using the Christoffel-Darboux formula. The close agreement suggests that numerical errors may be minimal.

whenever the measure is symmetric. Figure 14 shows a plot of the difference between Dirichlet Kernels calculated using the two different formulas. The small difference indicates that numerical errors are likely not impacting the calculations.

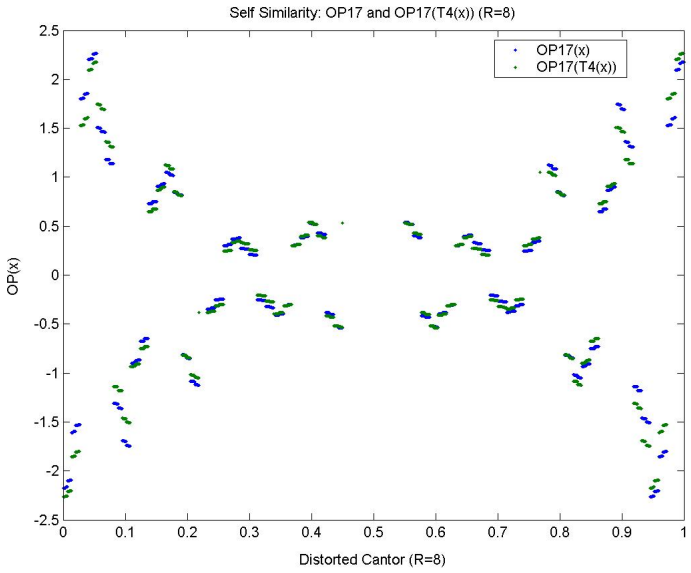

Figure 15: Plot of $P_{17}(x)$ and $P_{17}(T_4(x))$ with R=8, where $T_m(x)$ is a function that flips the first m bits of a binary number. In this case the Cantor set is thought of as a sequence of points that have binary addresses. Based on experimental determination, it appears that such an approximate equality holds for all $P_{2n+1}(x)$ such that $n = 2^k$ (using T_{k+1}).

Figure 15 displays an interesting self-similarity property of the CLPs. If we look at the points in the truncated Cantor set as binary addresses, then we can define the function T_m that flips the first m bits of a binary number and acts on the Cantor set. For example, T_1 corresponds to swapping the left half of the Cantor set for the Right half. We experimentally determined the approximate equality $P_{2^{k-1}+1}(x) \cong P_{2^{k-1}+1}(T_k(x))$.

Instead of looking at the polynomials as a function of x, it is possible to think of them as a function of n by fixing a value of x and letting the index be the variable. Figure 16 is an example of this with R=8 plotting $P_n(4097)$ vs. n. 4097 is the binary address of the leftmost point in the right half of the Cantor Set. What is interesting is that there seems to be a forbidden zone around zero. Perhaps the values of $P_n(4097)$ lie in some form of modified Cantor Set. The large gap around zero seems to support this conjecture.

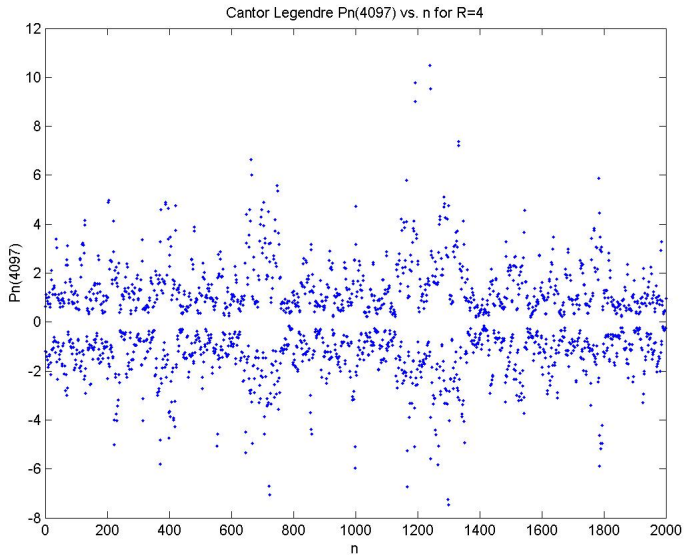

Figure 16: Plot of $(n, P_n(4097))$ where $R = 8$ and 4097 is the binary address of the left most element in the right half of the Cantor Set.

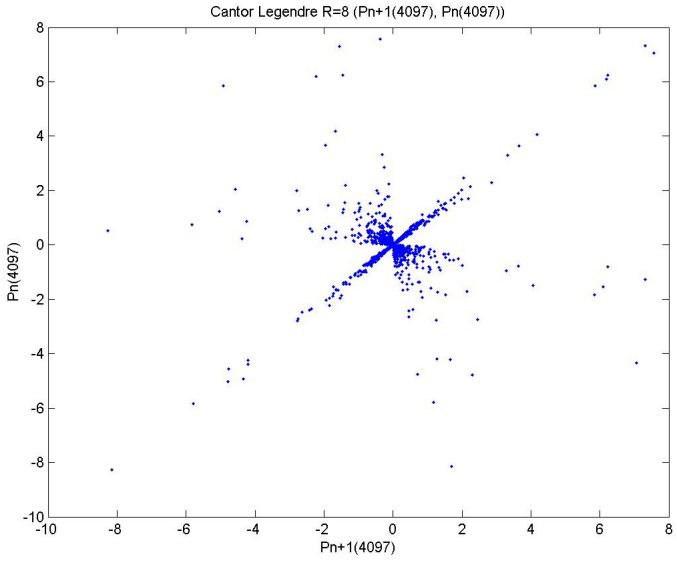

Figure 17: Plot of $(P_{n+1}(4097), P_n(4097))$ where $R = 8$ and 4097 is the binary address of the left most element in the right half of the Cantor Set.

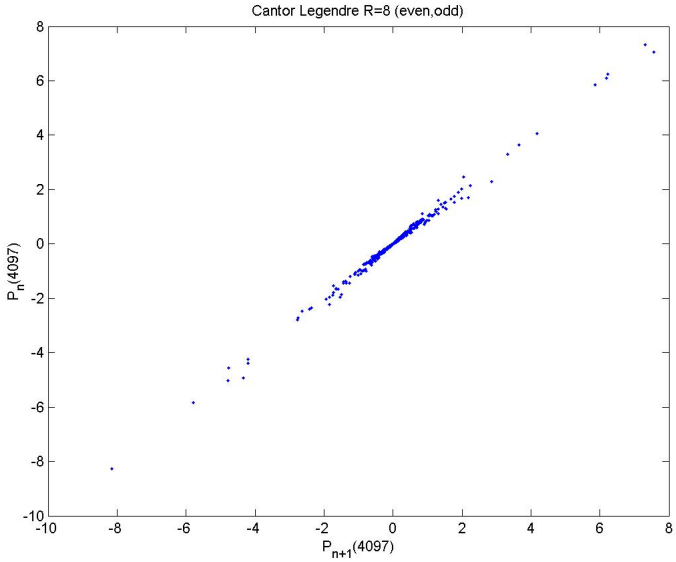

Figure 18: Plot of $(P_{n+1}(4097), P_n(4097))$ where $R = 8$ and 4097 is the binary address of the left most element in the right half of the Cantor Set, except this time n is incremented by 2 such that only the odd polynomials appear on the y-axis and only the even on the x-axis.

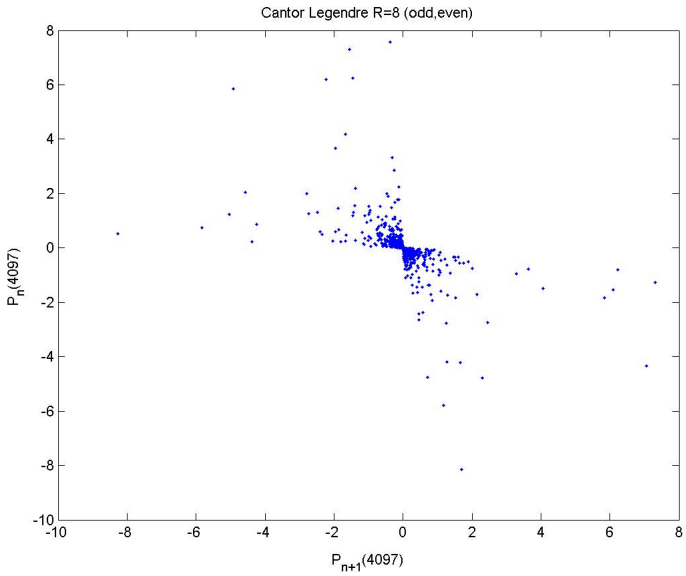

Figure 19: Plot of $(P_{n+1}(4097), P_n(4097))$ where $R = 8$ and 4097 is the binary address of the left most element in the right half of the Cantor Set, except this time n is incremented by 2 such that only the even polynomials appear on the y-axis and only the odd on the x-axis.

Another possibility is to plot vectors $(P_{n+1}(x), P_n(x))$. Figures 17,18 and 19 give examples of this with R=8. It is clear that there is a large amount of structure to the resulting plots.

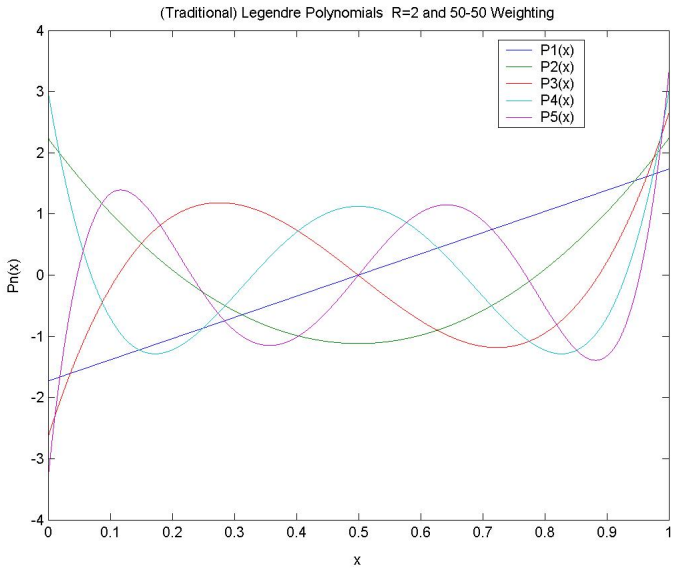

Figure 20: Plot of $P_n(x)$ on the unit interval with weighting 50 percent-50 percent (the unit interval). This gives the Legendre Polynomials.

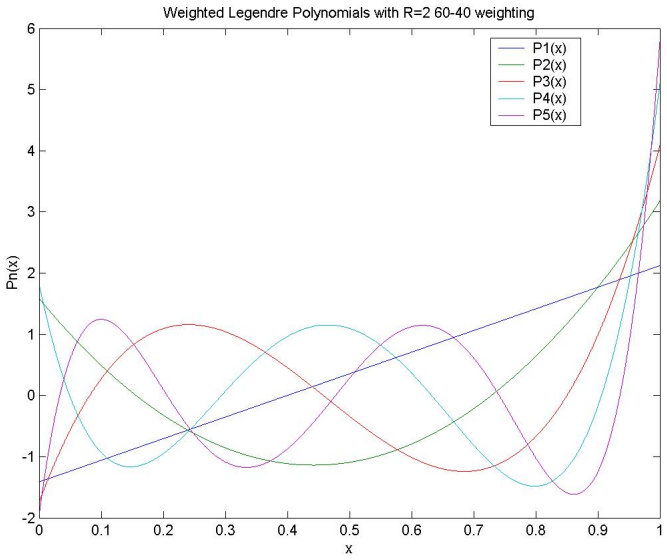

Figure 21: Plot of $P_n(x)$ on the unit interval with weighting 60 percent-40 percent.

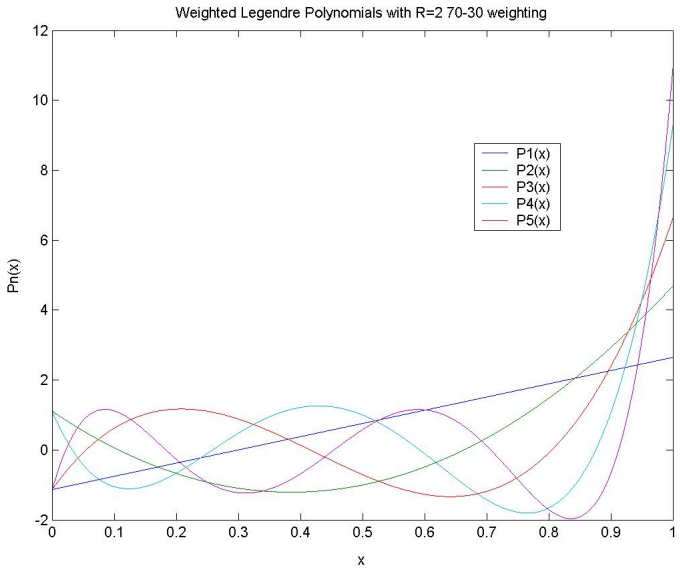

Figure 22: Plot of $P_n(x)$ on the unit interval with weighting 70 percent-30 percent.

Figure 20 shows the first several Legendre polynomials which are constructed using an even weighting to reproduce the unit interval. Figures 21 and 22 show the first several Weighted Legendre Polynomials (WLP) for the cases with asymmetric weighting $60\% - 40\%$ and $70\% - 30\%$. Figures 23 and 24 show some WLPs for larger values of n. In many ways the WLPs greatly resemble the legendre polynomials, but one notable exception is near zero; the WLPs remain bounded near zero, whereas the Legendre polynomials go to infinity.

Continuing with the idea of looking at the orthogonal polynomials as functions of index, figure 25 is a plot of $WLP_n(1)$ vs. n. For the Legendre polynomials there is a characteristic growth proportional to the $\sqrt{n}$. This fact holds with great accuracy for the weights 60-40, 65-45 and 70-30 as well. Figure 26 is a plot of $WLP_n(0)$ vs. n. An interesting periodic pattern is observed for all 3 weights with the same period but a small phase shift.

Figures 27, 28 and 29 are a plot of $WLP_n(.5)$ vs. n for the weights $60\% - 40\%$ and $70\% - 30\%$. In both cases we observe an oscillation in sign. Also, in both cases there exist 4 distinct curves corresponding to n of the form $n = 4k$, $n = 4k + 1$, $n = 4k + 2$ and $n = 4k + 3$ which can be seen in figures 31-34. Figure 34 is a plot of the vectors $(LP_{n+1}(.1), LP_n(.1))$ (the weighting is 50-50). This graph is an ellipse which is characteristic of the Legendre Polynomials for any x chosen. This can be derived by using the following asymptotic expansion for the Legendre Polynomials:

$$P_n(\cos\theta) \approx \sqrt{\frac{2n+1}{\pi n \sin\theta}} \sin\left((n+\frac{1}{2})\theta + \frac{\pi}{4}\right) \tag{9}$$

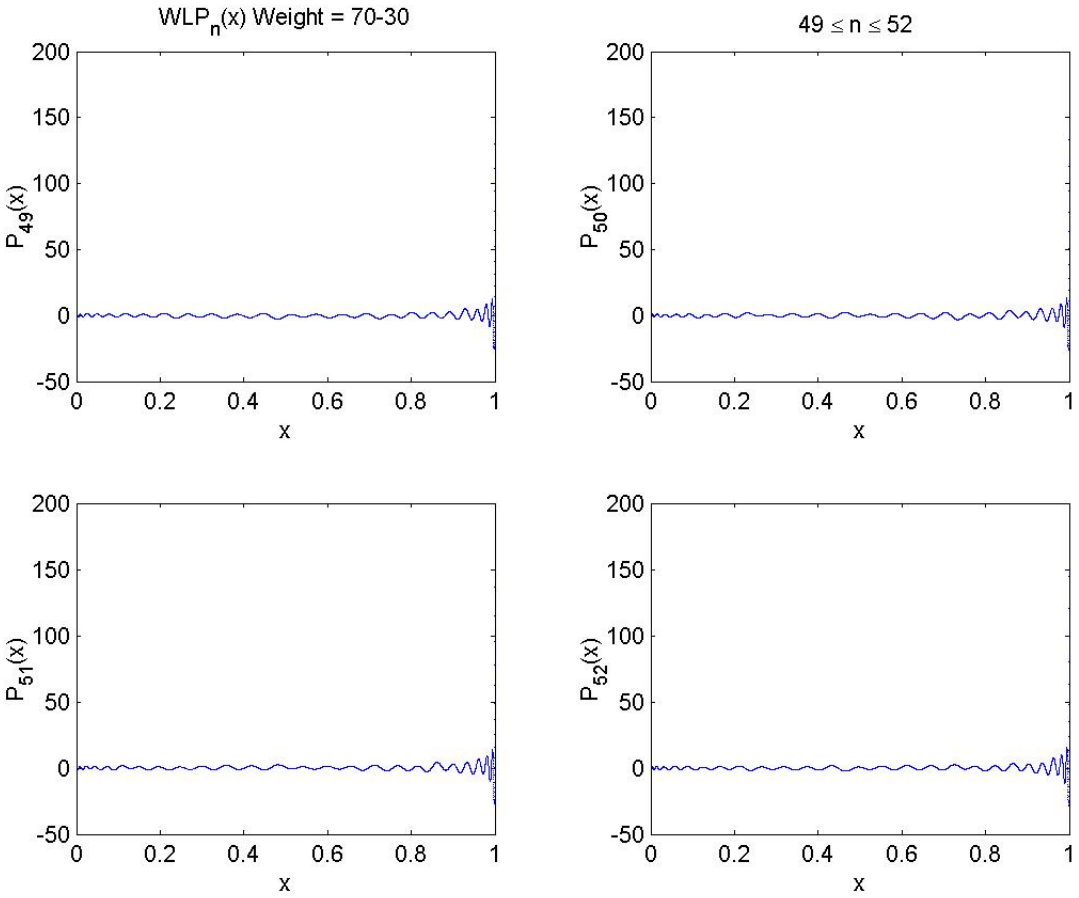

Figure 23: Plot of $P_n(x)$ on the unit interval with weighting 70 percent-30 percent for $49 \leq n \leq 52$.

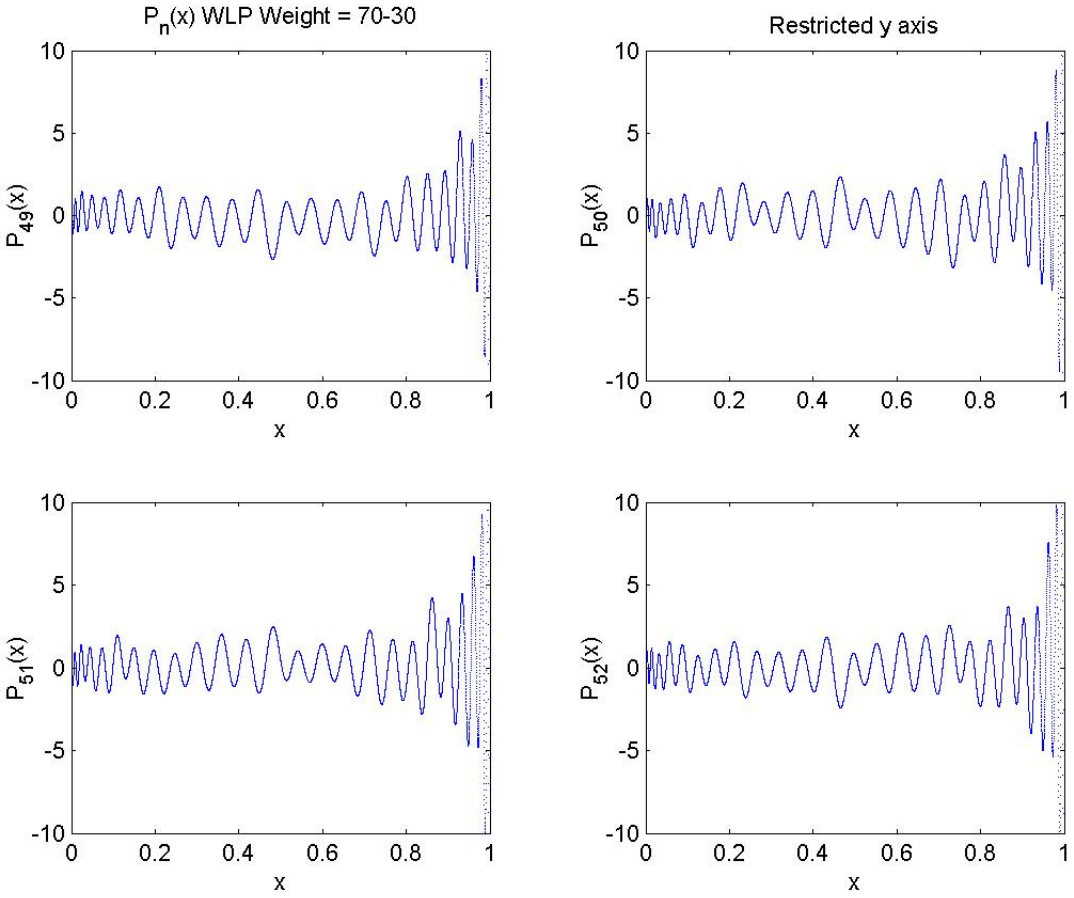

Figure 24: Plot of $P_n(x)$ on the unit interval with weighting 70 percent-30 percent for $49 \leq n \leq 52$ with the y-axis restricted to the range -10 to 10.

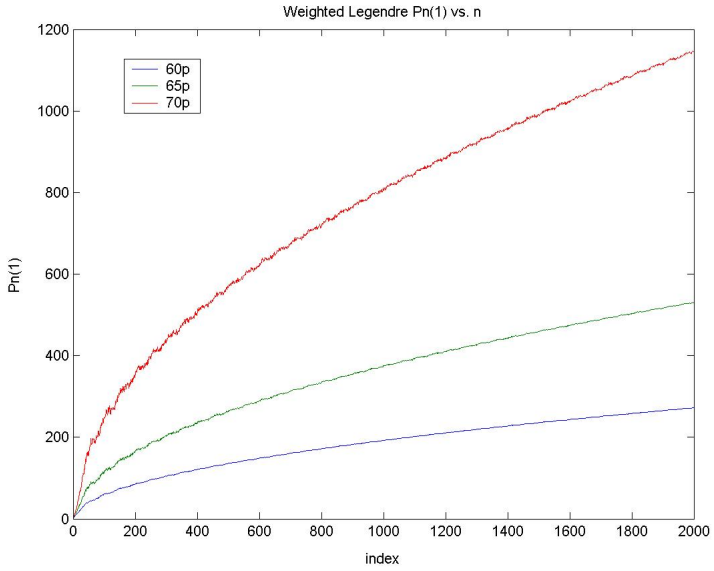

Figure 25: Plot of $P_n(1)$ vs. index. For all 3 weights the growth is proportional to the square root of n, which is characteristic of the traditional Legendre Polynomials.

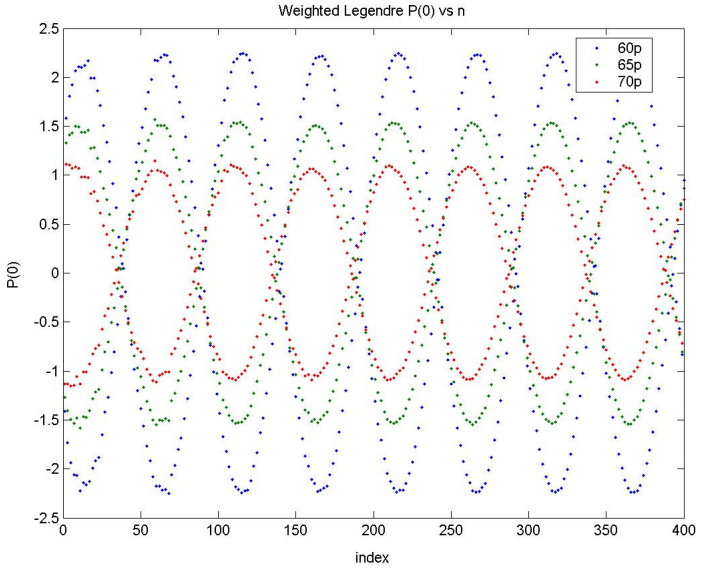

Figure 26: Plot of $P_n(0)$ vs. index. The values are periodic with essentially the same frequency (small phase shift) for all 3 weights.

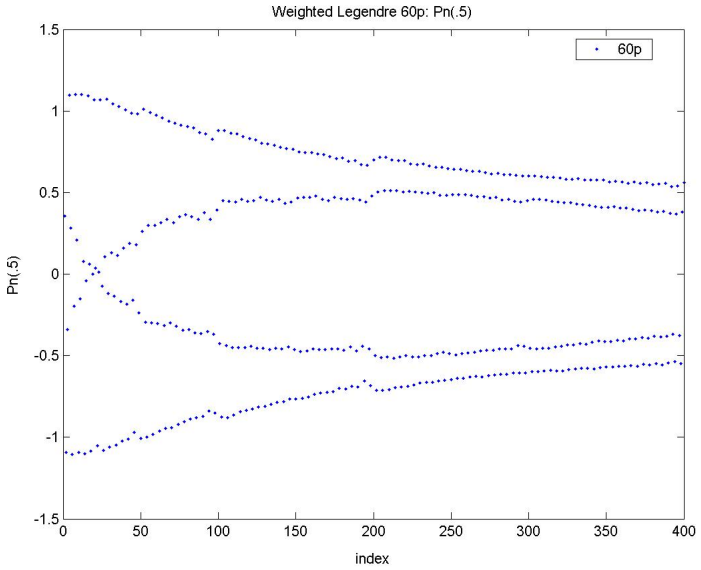

Figure 27: Plot of $P_n(.5)$ vs. index for weighting 60 percent left and 40 percent right. The values oscillate in sign between adjacent points.

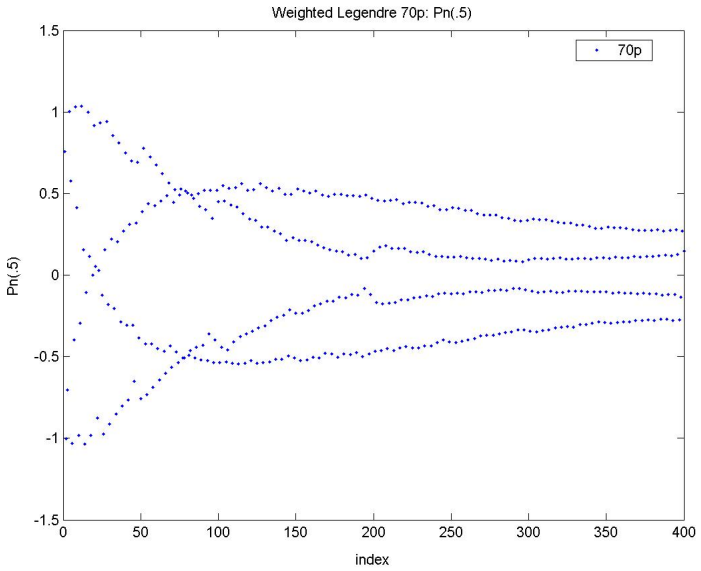

Figure 28: Plot of $P_n(.5)$ vs. index for weighting 70 percent left and 30 percent right.

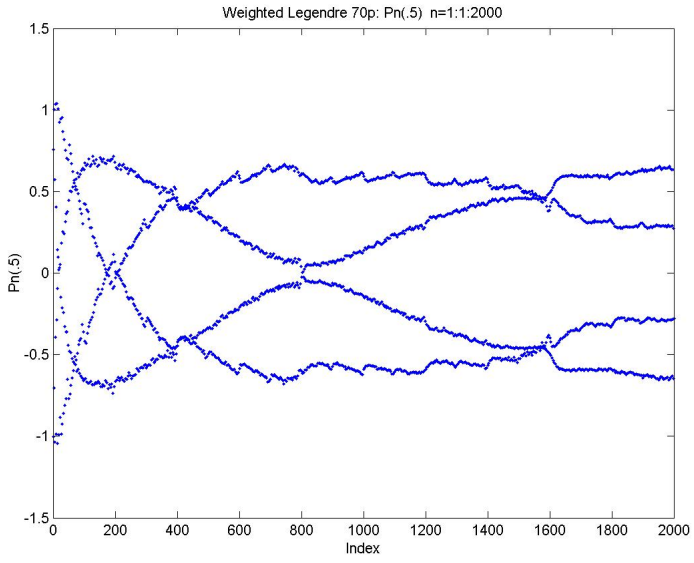

Figure 29: Plot of $P_n(.5)$ vs. index for weighting 70 percent left and 30 percent right for larger values of n.

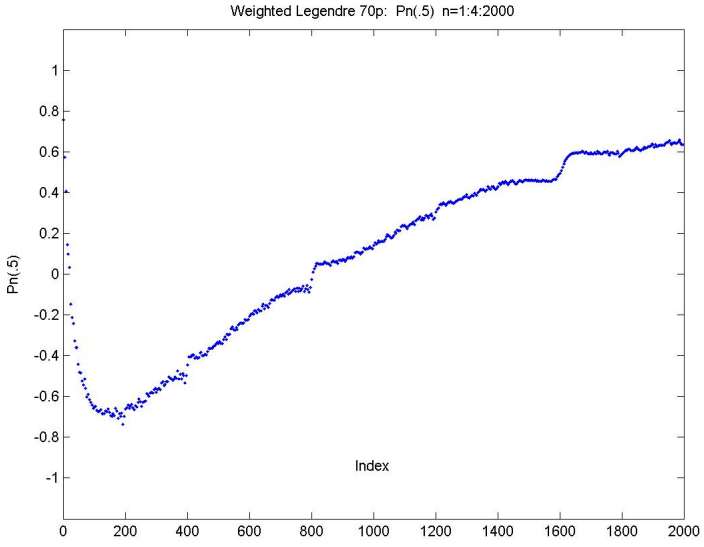

Figure 30: Plot of $P_n(.5)$ vs. index for weighting 70 percent left and 30 percent right for n a multiple of 4.

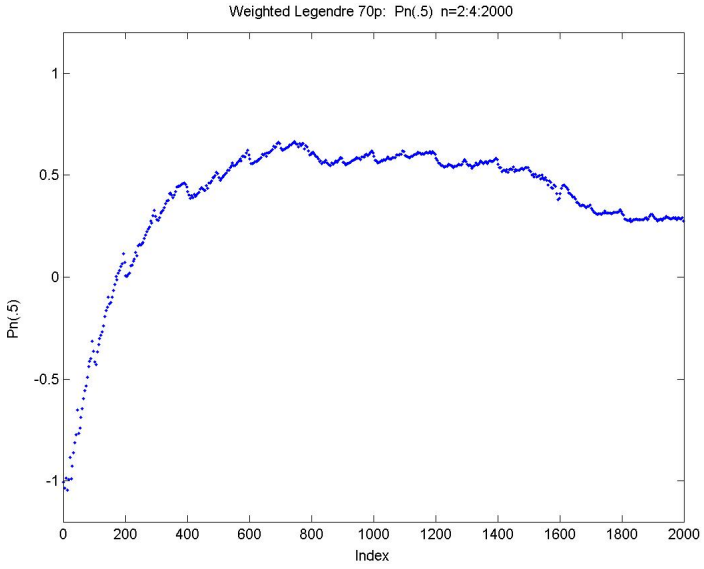

Figure 31: Plot of $P_n(.5)$ vs. index for weighting 70 percent left and 30 percent right for n of the form $n = 4k + 1$.

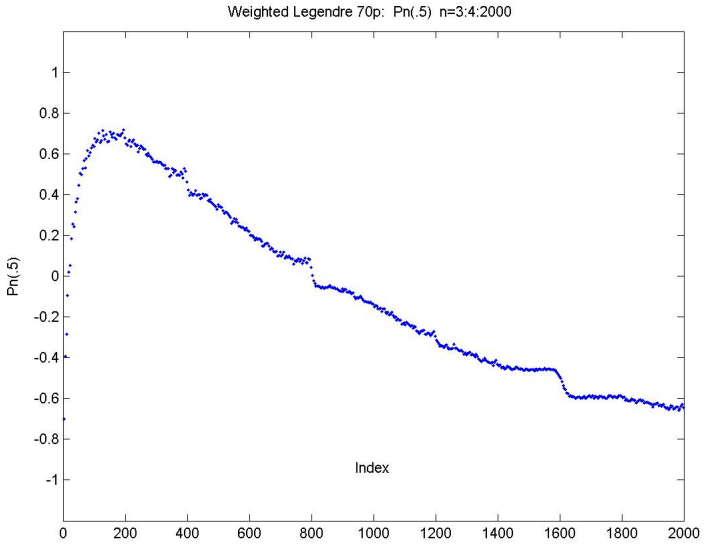

Figure 32: Plot of $P_n(.5)$ vs. index for weighting 70 percent left and 30 percent right for n of the form $n = 4k + 2$.

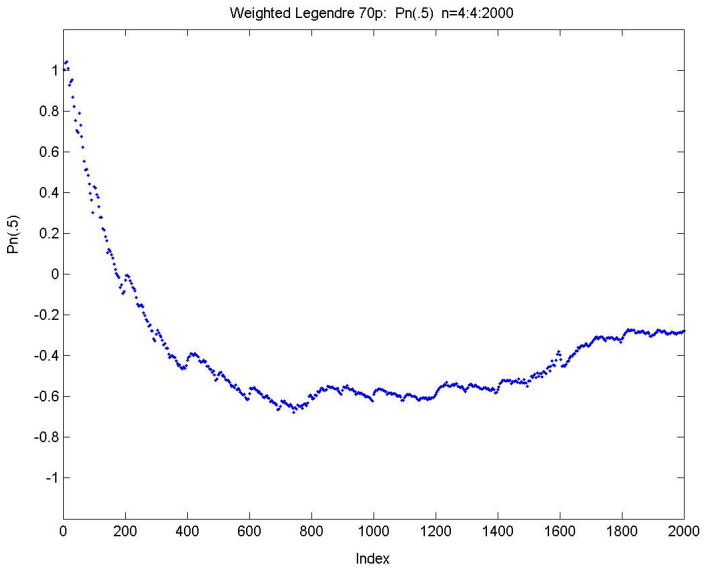

Figure 33: Plot of $P_n(.5)$ vs. index for weighting 70 percent left and 30 percent right for n of the form $n = 4k + 3$.

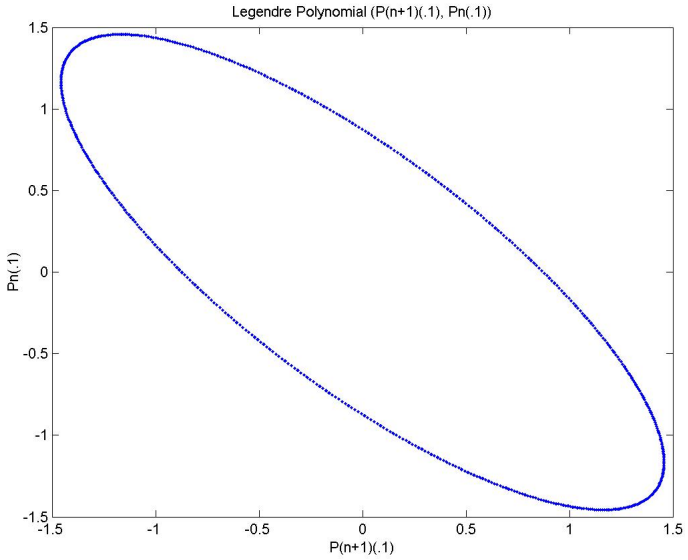

Figure 34: Plot of $P_n(.1)$ vs. $P_{n+1}(.1)$ $400 \leq n \leq 2000$ for Legendre Polynomials (weighting 50 percent left and 50 percent right). This ellipse is characteristic of the Legendre Polynomials.

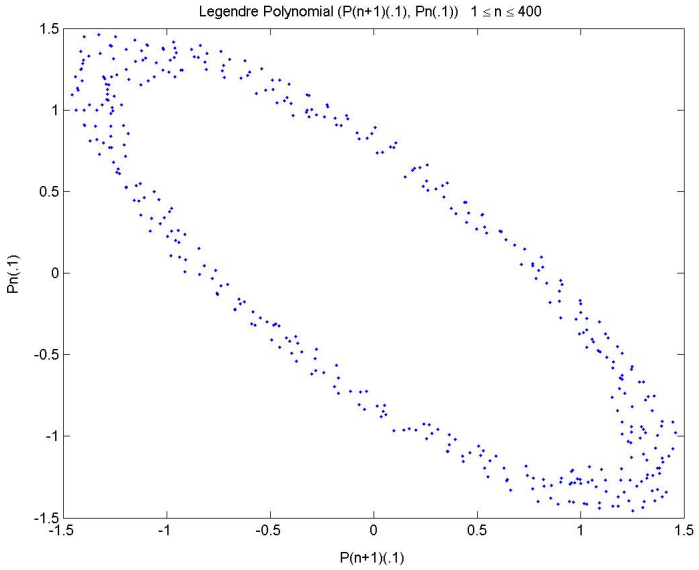

Figure 35: Plot of $P_n(.1)$ vs. $P_{n+1}(.1)$ $1 \leq n \leq 400$ for Weighted Legendre Polynomials with weighting 60 percent left and 40 percent right).

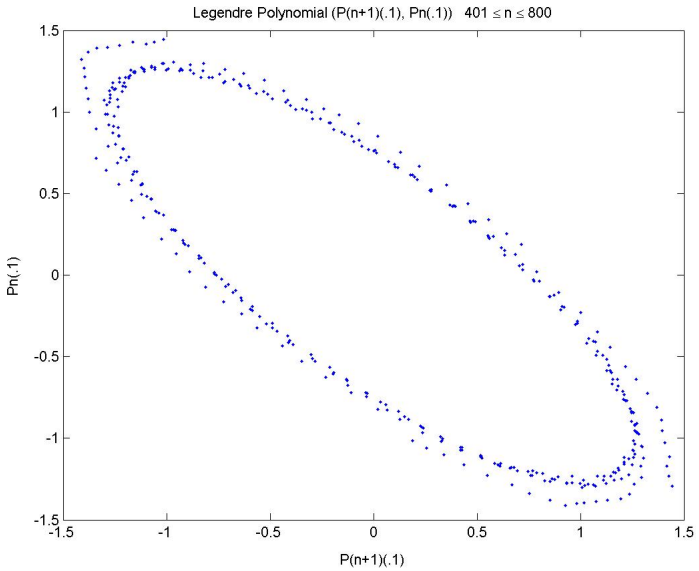

Figure 36: Plot of $P_n(.1)$ vs. $P_{n+1}(.1)$ $401 \leq n \leq 800$ for Weighted Legendre Polynomials with $P_1 = .6$. This better approximates an ellipse than figure 35 and indicates that the approximation improves for larger values of n.

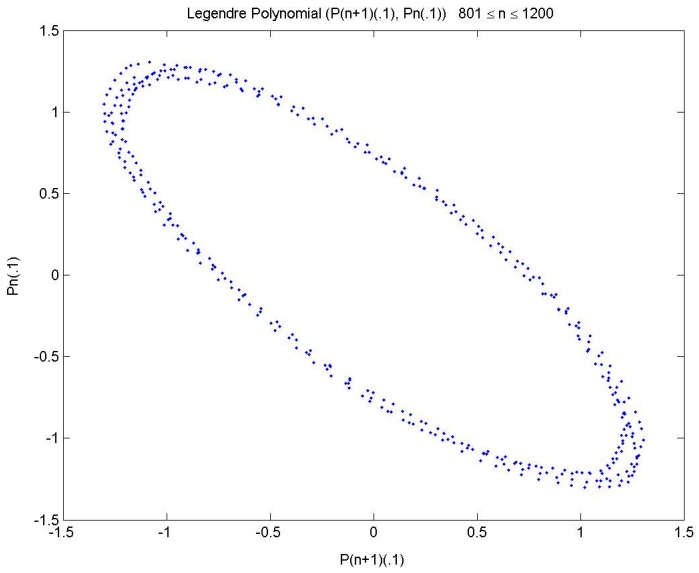

Figure 37: Plot of $P_n(.1)$ vs. $P_{n+1}(.1)$ $801 \leq n \leq 1200$ for Weighted Legendre Polynomials with $P_1 = .6$.

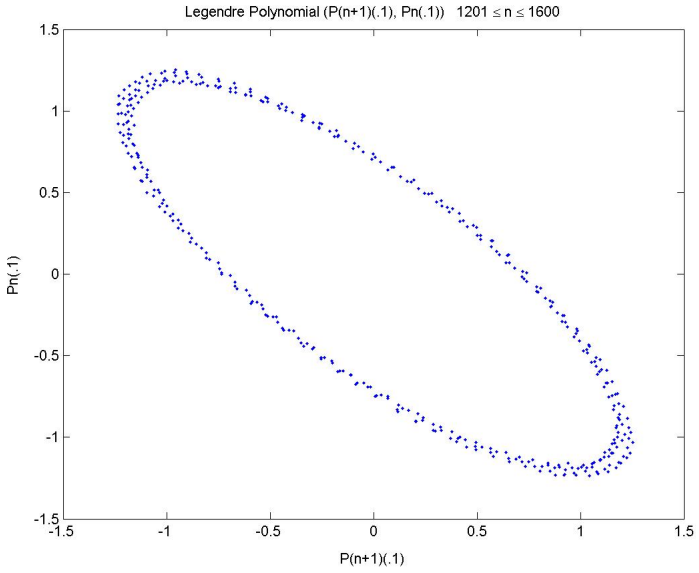

Figure 38: Plot of $P_n(.1)$ vs. $P_{n+1}(.1)$ $1201 \leq n \leq 1600$ for Weighted Legendre Polynomials with weighting $P_1 = .6$.

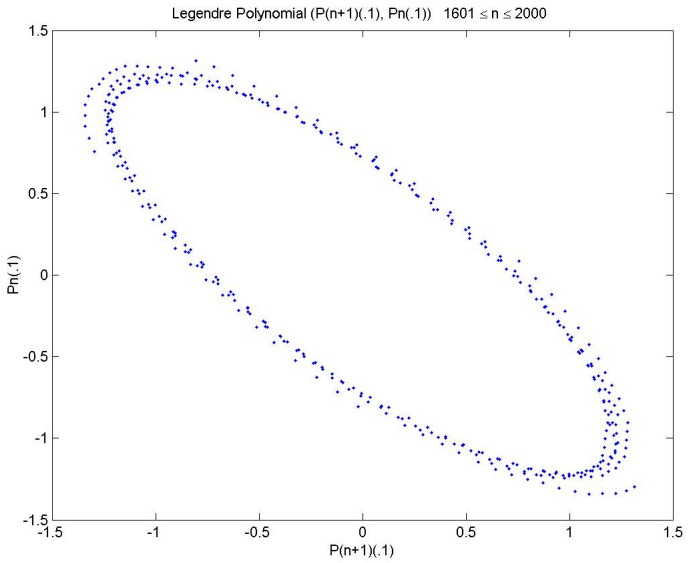

Figure 39: Plot of $P_n(.1)$ vs. $P_{n+1}(.1)$ $1601 \leq n \leq 2000$ for Weighted Legendre Polynomials with weighting $P_1 = .6$.

For a given θ if we denote $\sqrt{\frac{2n+1}{\pi n \sin\theta}}$ as C and $(n+\frac{1}{2})\theta + \frac{\pi}{4}$ as A_n then (9) becomes

$$P_n(\cos\theta) \approx C\sin(A_n) \tag{10}$$

where C has negligible n dependence for sufficiently large values of n and therefore all the n dependence resides in the A_n. We can now compute $(P_n, P_n+1) = (x, y)$. $P_n = x$ is simply $C\sin(A_n)$. To calculate $P_{n+1} = y$ notice that $A_{n+1} = A_n + \theta$ and then use the trig identities $\sin(A_n+\theta) = \sin(A_n)\cos(\theta) + \cos(A_n)\sin(\theta)$ and $\cos(A_n) = \pm\sqrt{1-\sin^2}A_n$; then $y = C(\cos\theta\sin A_n \pm \sin\theta\sqrt{1-\sin^2}A_n)$. We can then plug $\sin(A_n) = \frac{x}{c}$ into the equation for y to get:

$$\begin{aligned} y &= x\cos\theta \pm \sin\theta C\sqrt{1-\frac{x^2}{c^2}} \\ (y - x\cos\theta) &= \pm\sin\theta C\sqrt{1-\frac{x^2}{c^2}} \\ y^2 - 2xy\cos\theta + x^2 &= C^2\sin^2\theta \end{aligned} \tag{11}$$

where (10) is the equation of an ellipse for any θ in $(0, \pi)$ which corresponds to the unit interval when $x = \cos\theta$. The ellipse degenerates to a straight line when $\theta = 0$ or $\theta = \pi$.

Figure 35 is a similar plot but of $(WLP_{n+1}(.1), WLP_n(.1))$ with the weighting 60-40. This plot is an approximation to an ellipse and as we increase n in Figures 36-38 this approximation appears to improve. Unfortunately, Figure 39 with the highest n values deviates more than Figure 38 making it difficult to assert that as n goes to infinity we recover the ellipse of the Legendre Polynomials.

Conclusion

We have seen that there are a variety of interesting properties to the Cantor Legendre and the Weighted Legendre Polynomials. It remains to determine which of these experimental observations can be analytically proven, and to supply the proofs.

References

[G] W. Gautschi, Orthogonal Polynomials, Computation and Approximation, Oxford Univ. Press, 2004

[M1] G. Mantica (1996): *A Stable Stieltjes Technique for Computing Orthogonal Polynomials and Jacobi Matrices Associated with a Class of Singular Measures.*Constr. Approx. 12: 509-530.

[M2] G. Mantica (2000): *On computing Jacobi matrices associated with recurrent and Mobius iterated function systems.*Journal of Comp. and Applied Math. 115: 419-431.

[OS] P. Owrutsky and R. Strichartz, Orthogonal Polynomials with respect to Self-Similar Measures (Pending)

[SZ] G. Szego, Orthogonal polynomials (Fourth ed.), AMS Colloquium Publications 23 (1975), Amer. Math. Soc., Providence, RI.